Journal of Alloys and Compounds 513 (2012) 130–134

Contents lists available at SciVerse ScienceDirect

Journal of Alloys and Compounds

journal homepage: www.elsevier.com/locate/jallcom

Electrical characterization of DC sputtered ZnO/p-Si heterojunction

Yusuf Selim Ocak*

Department of Science, Faculty of Education, Dicle University, Diyarbakir, 21280, Turkey

ARTICLE INFO

Article history:
Received 26 April 2011
Received in revised form 2 October 2011
Accepted 3 October 2011
Available online 17 October 2011

Keywords:
Zinc oxide
Sputtering
Heterojunction
Electrical properties
Photoelectrical properties

ABSTRACT

ZnO thin films were formed on a p-Si semiconductor and a glass by DC sputtering technique. The ZnO films were analyzed using UV–vis spectroscopy and X-ray diffraction (XRD). Electrical and photoelectrical parameters of ZnO/p-Si heterojunction were determined by current–voltage (*I–V*), capacitance–voltage (*C–V*) and capacitance–frequency (*C–f*) of the device in dark and under the light with 100 mW/cm^2 and AM 1.5 illumination property. The device had a good rectifying property with 1.35 ideality factor, 0.76 eV barrier height and 6.69 kΩ series resistance values. It was seen that *I–V*, *C–V* and *C–f* measurements of the heterojunction had good sensitivity to the light and the device behaves as a photodiode and a photocapacitor.

1. Introduction

Zinc oxide (ZnO), a binary II–IV compound, is one of the important n-type semiconducting materials with 3.37 eV direct band gap and high transparency. Chemical and thermal stability and strong anti-radiation damaging ability are important parameters which make ZnO as an attractive material in device physics [1,2]. ZnO thin films have been widely studied because of their potential applications such as gas sensors, solar cells, optoelectronic devices, transparent conducting electrodes and optical waveguides [3–7].

ZnO thin films can be deposited on different substrates using many kinds of techniques including chemical vapor deposition, spray pyrolysis, electrodeposition, pulsed laser deposition and DC and RF magnetron sputtering [8–16]. For instance, Bacaksiz et al. [9] have formed ZnO thin films using zinc chloride, zinc acetate and zinc nitrate precursors by spray pyrolysis technique on glass substrates and determined their structural and optical properties by X-ray diffraction (XRD), scanning electron microscope (SEM) and optical transmittance spectra.

Recently, quite a lot of research groups have devoted to fabrication of ZnO based junctions due to potential applications in optoelectronic devices [9,13,17–20]. For instance, a heterojunction composed of n-type Al-doped ZnO and p-type Si has been fabricated by the laser molecular beam epitaxy (LMBE) technique and its photovoltaic properties have been studied at room temperature by Wang et al. [17]. They have shown that Al-doped ZnO/Si heterojunction has a great potential application in the wide-band photodetectors from ultraviolet to near infrared.

Sputtering technique is extensively used to deposit thin films in very large scale integration fabrication. The technique can offer uniform thickness over large wafers. Therefore, in this study, ZnO thin films were formed on a p-Si wafer and a glass to analysis the optical band gap and morphological properties of ZnO thin film formed by DC sputtering technique. Then, the electrical and photoelectrical properties of a ZnO/p-Si heterojunction were examined using current–voltage (*I–V*), capacitance–voltage (*C–V*) and capacitance–frequency (*C–f*) measurements in dark and under 100 mW/cm^2 and AM 1.5 illumination condition.

2. Experimental procedures

2.1. Formation of ohmic contact to p-Si wafer

A p-type Si wafer with (1 0 0) orientation and 1–10 Ω cm resistivity was used in the experiment. The wafer was boiled in trichloroethylene for 5 min and rinsed in acetone and isopropanol by ultrasonic vibration. It was etched by a solution of H_2O/HF (10:1) for 30 sn to remove the native oxide layer on wafer. Preceding each step, the wafer was rinsed in deionized water. It was dried under N_2 atmosphere and inserted into a deposition chamber immediately after the etching procedure. Al is one of the good choices to make an ohmic contact to p-Si [21]. Therefore, the ohmic contact was made by sputtering 250 nm Al on the back side of the wafer, then annealing at 450 °C for 15 min in a N_2 atmosphere.

2.2. Formation of ZnO thin film on p-Si wafer and a glass

A ZnO target bought from Kurt J. Lesker Company with a diameter of 2 in. was used for sputtering procedures. Before the formation of ZnO thin films, the front side of p-Si wafer was etched by a solution of H_2O/HF (10:1) and dried under N_2 atmosphere. Moreover, a glass was rinsed in acetone and isopropanol by ultrasonic vibration and dried under N_2 atmosphere. After the cleaning procedures the wafer and the glass were immediately inserted into a vacuum chamber. The chamber,

* Tel.: +90 412 248 80 30x8889; fax: +90 412 248 82 57.
E-mail address: yusufselim@gmail.com

0925-8388/$ – see front matter © 2011 Elsevier B.V. All rights reserved.
doi:10.1016/j.jallcom.2011.10.005

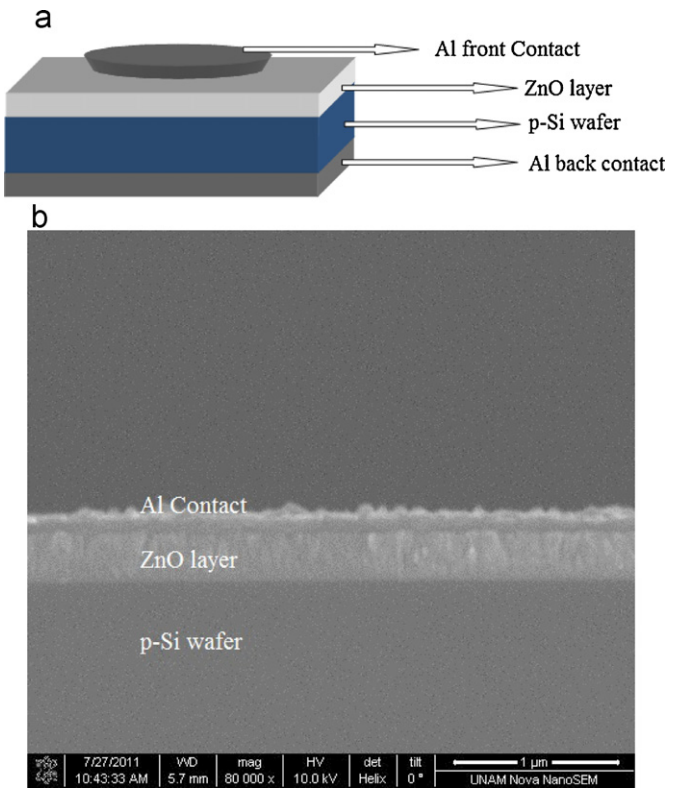

Fig. 1. (a) The schematic diagram of Al/ZnO/p-Si/Al structure and (b) the SEM image of the cross section of Al/ZnO/p-Si structure.

firstly, was down to about 10^{-6} Torr. Ar gas was introduced into the chamber and the sputtering was performed with about 1.2 Å/s speed at 5×10^{-3} Torr. The displacement between the target and substrate was about 10 cm, target and substrate were parallel to each other and the applied power to the target was 40 W during the sputtering process.

2.3. Analysis of ZnO thin Films

XRD measurement of the ZnO film on p-Si wafer was carried out by using a Rigaku Miniflex XRD system equipped with Cu Kα radiation of average wavelength of 1.54059 Å within the angle range 2θ: 10–60°. UV–vis spectrometry was taken using a Perkin Elmer Lambda 25 UV–vis spectrophotometer in order to see the transmittance of ZnO thin film and calculate the optical band gap of the film on glass.

2.4. Formation of an Al front contact and taking electrical measurements of the device

After analyzing the ZnO thin films, Al was thermally evaporated using a shadow mask in the vacuum system at 3×10^{-6} Torr. The diameter of circular Al contacts was 1.5 mm. The thicknesses of ZnO layer and Al contact were determined as 270 and 140 nm, respectively, using FEI Nova NanoSEM 430. The schematic diagram and the cross section of Al/ZnO/p-Si structure obtained using FEI Nova NanoSEM 430 are shown in Fig. 1a and b, respectively. The current–voltage (I–V) measurements were performed by Keithley 2400 sourcemeter and C–V measurements were executed by Agilent HP 4294A impedance analyzer (40 Hz–110 MHz). Photoelectrical measurements were performed under a solar simulator with 100 mW/cm^2 illumination and AM 1.5 global filter

3. Results and discussion

3.1. Analyze of DC sputtered ZnO thin films

To analyze the ZnO thin film on p-Si wafer, firstly, XRD measurements were obtained. Fig. 2 shows the XRD pattern of ZnO thin film within the 2θ range of 10–60°. As it is seen from the figure, there is only a strong peak at 34.05°. It implies the (0 0 2) orientation which is preferable orientation for ZnO films [9].

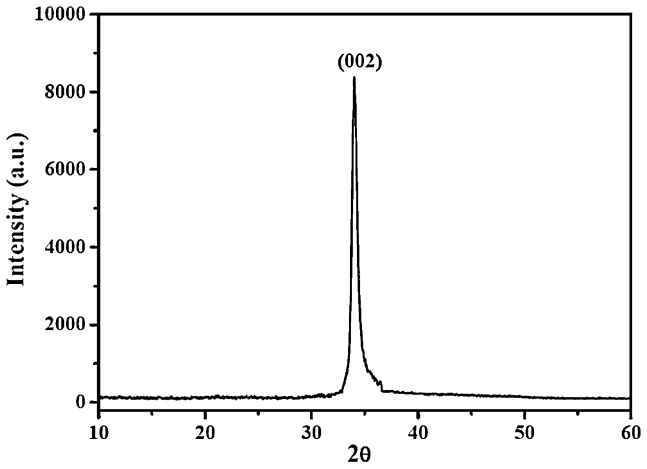

Fig. 2. XRD pattern of the ZnO thin film on a p-Si wafer within the 2θ range of 10–60°.

Fig. 3a presents the optical transmittance spectra of the ZnO thin film observed at room temperature. The film is transparent to visible light and the optical transmittance values of films vary between 70 and 87% in visible region. The optical band gap (E_g) of the film formed on the glass can be calculated using the equation;

$$\alpha h\upsilon = B(h\upsilon - E_g)^m \quad (1)$$

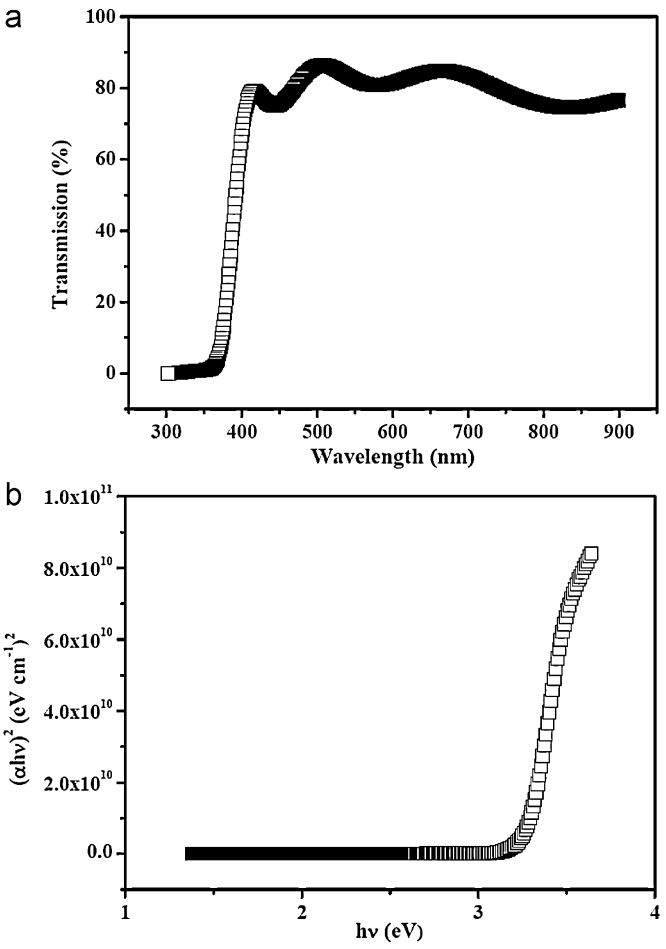

Fig. 3. (a) The optical transmittance spectra and (b) $(\alpha h\nu)^2$–$h\nu$ curve of the ZnO thin film on a glass.

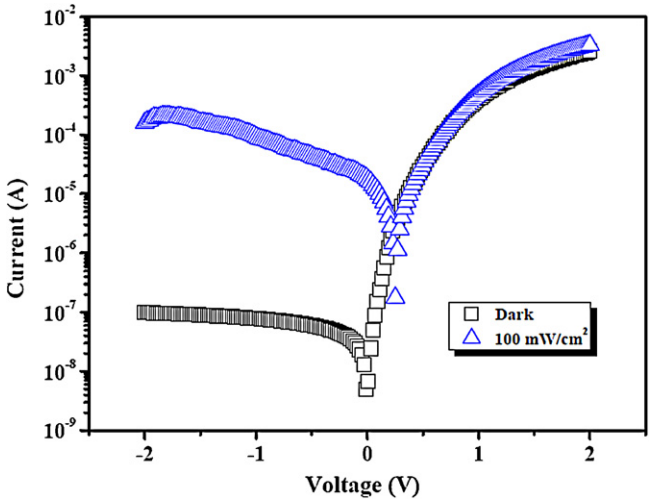

Fig. 4. *I–V* characteristics of the Al/ZnO/p-Si diode in dark and under a solar simulator.

where α is the absorption coefficient, B is a constant and h is the plank constant. The exponent m depends on the nature of the transition, $m = 1/2$, 2, 3/2, or 3 for allowed direct, allowed nondirect, forbidden direct, or forbidden nondirect transitions, respectively [22,23]. It is well known that ZnO has an allowed direct band gap and $m = 1/2$ was used for the band gap calculation. Fig. 3b shows $(\alpha h\nu)^2$–$h\nu$ curve of ZnO thin film on glass according to Eq. (1). The E_g of ZnO thin film was determined as 3.28 eV by extrapolating the straight line of the graph to intercept the photon energy axis. The band energy of DC sputtered ZnO thin film was calculated as 0.09 eV smaller the one of ZnO single crystal (3.37 eV) [24]. The optical absorption at absorption edge corresponds to the transition from valence band to conduction band, while the absorption edge shifting to the lower energy relates to some local energy levels caused by some intrinsic defects [25]. Optical properties of ZnO thin films formed using different methods and conditions have been analyzed by some authors. For instance, Shan and Yu [26] have used pulsed laser deposition (PLD) technique to deposit pure and Al-doped ZnO thin films at different temperatures on glass substrates. They have shown that the optical band gap of Al-doped ZnO thin films ranging from 3.32 to 3.77 eV are higher than those of 3.25 to 3.28 eV obtained for pure ZnO thin films. Moreover, Mohanta and Pal [27] have formed junctions between two ZnO nanoparticles and they have reported that rectification is higher in nanodiodes with high bandgap nanoparticles.

3.2. Current–voltage properties of ZnO/p-Si structure

The current–voltage (I–V) characteristics of the device in dark and under a solar simulator are presented in Fig. 4. The weak voltage dependence of the reverse bias current and the exponential increase in the forward bias current are the characteristic properties of rectifying contacts. As it is seen from the figure the device has a good rectifying property in dark. The rectification ratio of the structure at ±1 V is about 1.4×10^4. It is assumed that the forward bias current of the device for $qV \gg 3kT$ is due to thermionic emission current and the net current of a diode with a series resistance can be expressed as [28]:

$$I = I_0 \exp\left(\frac{q(V - IR_S)}{nkT}\right) \tag{2}$$

where I_0 is the saturation current and written as

$$I_0 = AA^*T^2 \exp\left(-\frac{q\phi_b}{kT}\right) \tag{3}$$

where ϕ_b is the barrier height at zero bias, A is the diode area, A^* is the effective Richardson constant equals to 36 A cm^{-2} K^{-2} for ZnO [29] and n is the ideality factor.

The ideality factor of the diode was calculated as 1.35 from the slope of the linear region of Fig. 4 by the help of using the Eq. (2). The ideality factor of an ideal diode should be unity. The obtained n value of 1.35 implies deviation from ideal behavior which results from the presence of surface states in ZnO, oxide layer on silicon and series resistance of the diode [6]. I_0 is determined from the intercept of ln$I$ vs. V curve on the y-axis and the barrier height can be obtained from the equation:

$$q\phi_b = kT \ln\left(\frac{AA^*T^2}{I_0}\right) \tag{4}$$

The value of the ϕ_b was obtained from the I–V characteristics using Eq. (4) to be 0.76 eV. The current curve in the forward bias region becomes dominated by series resistance from contact wires or bulk resistance of semiconductors, giving rise to the curvature at high current in the ln$I$–V plot [30]. As known, the ideality factor n is a measure of conformity of the diode to pure thermionic emission. The ideality factor value of 1.35 which is much larger than 1.1 shows that the transport properties of the device are not well modeled by thermionic emission only. Thus the barrier height and ideality factor are merely a curve fitting parameter due to the rectifying properties of this sample and should not be interpreted as representing the true parameters [31]. The series resistance of the diode can be calculated by Norde functions [32] defined as

$$F(V) = \frac{V}{\gamma} - \frac{1}{\beta} \ln\left(\frac{I(V)}{AA^*T^2}\right) \tag{5}$$

where γ is the first integer than ideality factor, β is a temperature dependent value calculated with $\beta = q/kT$ and $I(V)$ is the current achieved from I–V data. γ value was taken as 2 for Al/ZnO/p-Si structure. After determining the minimum value of F vs V plot, the barrier height can be calculated from the equation

$$\phi_b = F(V_0) + \frac{V_0}{\gamma} - \frac{kT}{q} \tag{6}$$

where $F(V_0)$ is the minimum $F(V)$ value of F vs. V graph and V_0 is the corresponding voltage value. Fig. 5 shows the $F(V)$–V graph of the Al/ZnO/p-Si diode. The series resistance (R_S) of the junction can be defined through the relation

$$R_S = \frac{kT(\gamma - n)}{qI} \tag{7}$$

The $F(V_0)$ and V_0 values were determined as 0.71 V and 0.20 V, respectively. The values of ϕ_b and R_S were calculated as 0.79 eV and 6.69 kΩ, respectively.Very recently, similar studies have been carried out by different groups. For instance, Choi et al. [18] have fabricated vertical aligned p-Si nanowires (NW) by electroless wet chemical etching of Si wafer and deposited ZnO onto p-type Si NW arrays by RF sputtering technique to realize p-Si NWs/ZnO heterojunction. They have determined electrical characteristics of the device by I–V and C–V measurements. It has been shown that the structure has forward-to-reverse current ratio of 519 at 3.0 V and ideality factor of 4.5. Furthermore, Zebbar et al. [20] have prepared n-ZnO/p-Si have been heterojunction structures by ultrasonic spraying of undoped ZnO thin films onto p-type Si (1 0 0) substrates. They have reported the rectification ratio, ideality factor, barrier height and series resistance of the heterojunction as 36 at 3 V, 4, 0.67 eV and 4.8 kΩ, respectively.

Fig. 4 also presents the current–voltage characteristics of the diode under a simulator with 100 mW/cm^2 and AM 1.5 illumination condition. As seen from the figure the photocurrent in the ZnO/p-Si junction in reverse direction is strongly enhanced by photoillumination. This behavior gives information on the electron–hole pairs,

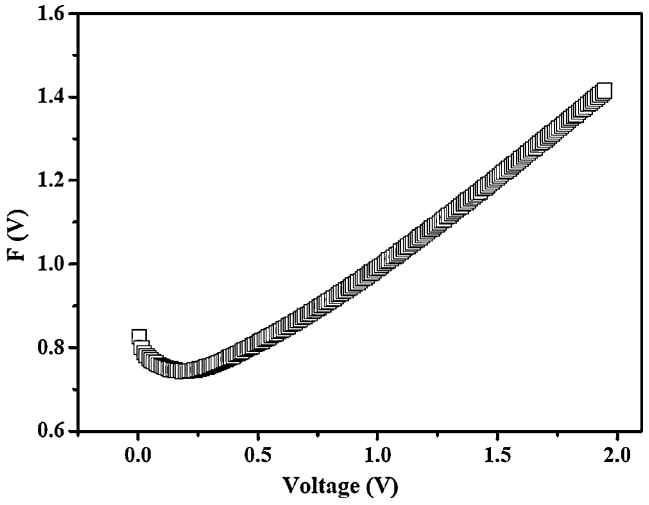

Fig. 5. $F(V)$–V plot for the Al/ZnO/p-Si diode.

which were effectively generated in the junction by incident photons [33,34]. The light increases the reverse bias I–V characteristics about 3200 times at −1 V. The maximum open circuit voltage (V_{OC}) and short-circuit current (I_{SC}) values for the diode were determined to be 251 mV and 19 μA, respectively. The photoelectric effect in the structure is because of the light-induced electron generation at the depletion region of the structure [33].

3.3. Capacitance–voltage and capacitance–frequency properties of ZnO/p-Si structure

Fig. 6a shows the capacitance–voltage (C–V) measurements of Al/ZnO/p-Si diode in dark and under 100 mW/cm^2 light at 500 kHz. The depletion region capacitance can be written as [28]

$$\frac{1}{C^2} = \frac{2(V_{bi} + V)}{q\varepsilon_S A^2 N_d} \tag{8}$$

where ε_S is the dielectric constant of ZnO (ε_S = 8.5) [35], V_{bi} is the diffusion potential at zero bias determined from the extrapolation of the linear reverse bias C^{-2}–V plot and N_d the donor concentration of ZnO. The C^{-2}–V plot of ZnO thin film obtained by DC sputtering technique is presented in Fig. 6b. The V_{bi} and N_d values were determined as 0.66 eV and 1.955×10^{16} cm^{-3}. The barrier height value can be determined from the relation:

$$\phi_{b(C-V)} = V_{bi} + \frac{kT}{q} \ln\left(\frac{N_c}{N_d}\right) \tag{9}$$

where N_c is the density of states in the conduction band ($N_c = 3.35 \times 10^{18}$ cm^{-3}) [36]. The barrier height of the diode was calculated using V_{bi} and N_d values using Eq. (8) and C^{-2}–V data as 0.79 eV. The barrier height value of the structure is 0.03 eV higher than the one obtained from I–V measurements. This discrepancy in the barrier height values obtained from I–V and C–V characteristics results from different nature of the measurement techniques. The capacitance is insensitive to potential fluctuations on a length scale of less than the space charge region and C–V method averages over the whole area and measures to describe the ϕ_b. The dc current across the interface depends exponentially on barrier height and thus sensitively on the detailed distribution at the interface [28,30].

As seen from Fig. 6a, C–V characteristics of the device are strongly affected from light. The increase in the capacitance is due to the illumination induced interface states and electron–hole pairs in the depletion region [37,38]. In addition, the capacitance–frequency (C–f) measurements in dark and under

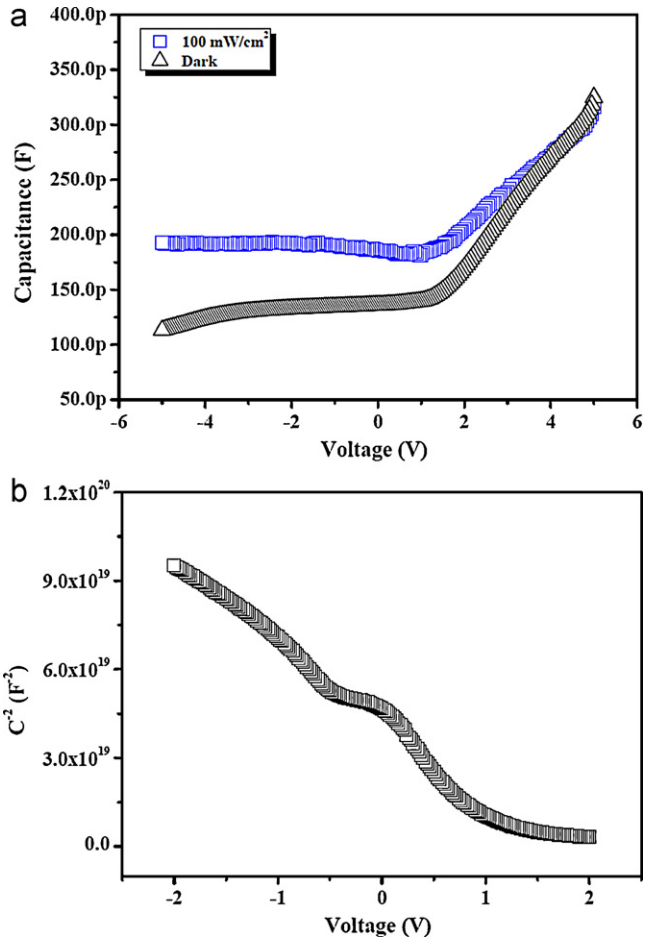

Fig. 6. (a) C–V measurements of the Al/ZnO/p-Si diode in dark and under illumination and (b) C^{-2}–V plot of the Al/ZnO/p-Si diode in dark.

illumination are presented in Fig. 7. The capacitance decreases with increasing frequency due to the presence of the interface states. The charges at the interface cannot follow the fast ac signal and they do not contribute to the diode capacitance. The increase in the capacitance under the light implies the photocapacitance behavior of the diode.

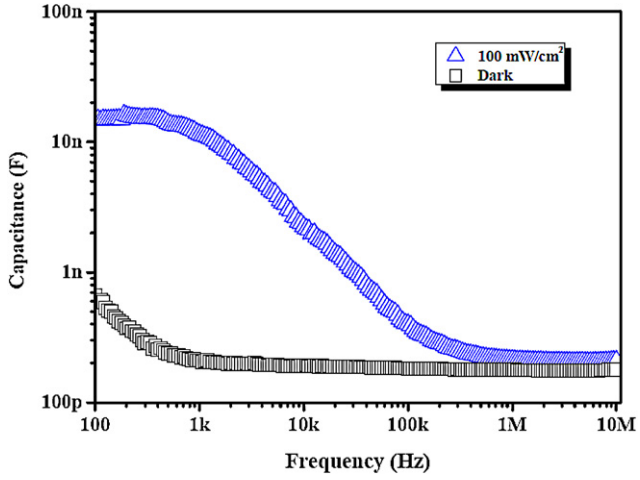

Fig. 7. C–f measurements of the Al/ZnO/p-Si diode in dark and under illumination.

4. Conclusions

DC sputtered ZnO thin films were formed on a glass and a p-Si wafer using a ZnO target. The optical and morphological properties of the films were studied. It was seen that the film had (0 0 2) orientation and 3.28 eV optical band gap. The electrical properties of an Al/ZnO/p-Si diode were analyzed using its *I–V*, *C–V* and *C–f* measurements in dark and under the light with 100 mW/cm^2 illumination. It was observed that the device had a good rectification and behaves as a photodiode and a photocapacitor.

Acknowledgements

The author would like to thank Prof. Dr. Rasit Turan and Mustafa Kulakci for their laboratory support.

References

[1] T. Wang, X. Diao, P. Ding, J. Alloys Compd. 509 (2011) 4910–4915.
[2] W. Gao, Z. Li, Ceram. Int. 30 (2004) 1155–1159.
[3] D.K. Kim, H.B. Kim, J. Alloys Compd. 509 (2011) 421–425.
[4] S.K. Sharma, A.I. Inamdar, H. Im, B.G. Kim, P.S. Patil, J. Alloys Compd. 509 (2011) 2127–2131.
[5] J. Chen, J. Li, J. Li, G. Xiao, X. Yang, J. Alloys Compd. 509 (2011) *740–743*.
[6] F. Yakuphanoglu, J. Alloys Compd. 494 (2010) 451–455.
[7] K.H. Lee, C.H. Park, K. Lee, T. Ha, J.H. Kim, J. Yun, G.H. Lee, S. Im, Org. Electron. 12 (2011) 1103–1107.
[8] J. Su, C. Wang, C. Tang, Q.N.Y. Zhang, F.u Zhuxi, J. Alloys Compd. 509 (2011) 6102–6105.
[9] E. Bacaksiz, M. Parlak, M. Tomakin, A. Ozcelik, M. Karakiz, M. Altunbas, J. Alloys Compd. 466 (2008) 447–450.
[10] S. Aydogan, K. Cinar, H. Asıl, C. Coskun, A. Turut, J. Alloys Compd. 476 (2009) 913–918.
[11] A. Kaushal, D. Kaur, J. Alloys Compd. 509 (2011) 200–205.
[12] C.W. Hsua, T.C. Cheng, C.H. Yangc, Y.L. Shen, J.S. Wu, S.Y. Wu, J. Alloys Compd. 509 (2011) 1774–1776.
[13] Z. Liang, X. Yub, B. Lei, P. Liua, W. Mai, J. Alloys Compd. 509 (2011) 5437–5440.
[14] C.E. Benouis, M. Benhaliliba, A.S. Juarez, M.S. Aida, F. Chami, F. Yakuphanoglu, J. Alloys Compd. 490 (2010) 62–67.
[15] M. Benhaliliba, C.E. Benouis, M.S. Aida, A. Sanchez Juarez, F. Yakuphanoglu, A. Tiburcio Silver, J. Alloys Compd. 506 (2010) 548–553.
[16] Y.S. Ocak, M. Kulakci, R. Turan, T. Kilicoglu, O. Gullu, J. Alloys Compd. 509 (2011) 6631–6634.
[17] S. Wang, M. Chen, X. Zhao, J. Chen, W. Yu, J. Wang, G. Fu, Physica B 405 (2010) 4966–4969.
[18] J.H. Choi, S.N. Das, K.J. Moon, J.P. Kar, J.M. Myoung, Solid State Electron. 54 (2010) 1582–1585.
[19] E. Bacaksiz, S. Aksu, G. Cankaya, S. Yilmaz, I. Polat, T. Kucukomeroglu, A. Varilci, Thin Solid Films 519 (2011) 3679–3685.
[20] N. Zebbar, Y. Kheireddine, K. Mokeddem, A. Hafdallah, M. Kechouane, M.S. Aida, Mater. Sci. Semicond. Process (2011), doi:10.1016/j.mssp.2011.03.001.
[21] S.M Sze, K.Ng Kwok, Physics of Semiconductor Devices, third ed., John Wiley & Sons, Inc., New Jersey, 2007.
[22] F. Yakuphanoglu, B.F. Senkal, A. Sarac, J. Electron. Mater. 37 (2008) 930–934.
[23] M. Cakar, O. Gullu, N. Yildirim, A. Turut, J. Electron. Mater. 38 (2009) 1995–1999.
[24] D.C. Look, Mater. Sci. Eng. B 80 (2001) 383.
[25] L. Zhao, J. Lian, Y. Liu, Q. Jiang, Appl. Surf. Sci. 252 (2006) 8451–8455.
[26] F.K. Shan, Y.S. Yu, J. Eur. Ceram. Soc. 24 (2004) 1869–1872.
[27] K. Mohanta, A.J. Pal, Nanotechnology 20 (2009) 185203.
[28] E.H. Rhoderick, R.H. Willams, Metal–Semiconductor Contacts, Clarendon, Oxford, 1988.
[29] O. Madelung, M. Schulz, H. Weiss, Semimagnetic Semiconductors, Landolt–Bornstein, New Series Group III, vol. 17, Part B, Springer, Berlin, 1982.
[30] O. Gullu, A. Turut, J. Appl. Phys. 106 (2009) 103717.
[31] S. Karatas, C. Temirci, M. Cakar, A. Turut, Appl. Surf. Sci. 252 (2006) 2209–2216.
[32] H. Norde, J. Appl. Phys. 50 (1979) 5052.
[33] A.A.M. Farag, J. Alloys Compd. 509 (2011) 8056–8064.
[34] T. Kilicoglu, Y.S. Ocak, Microelectron. Eng. 88 (2011) 150–154.
[35] C.W. Nahm, C.H. Park, J. Mater. Sci. 35 (2000) 3037.
[36] S.M. Sze, Physics of Semiconductor Devices, second ed., Wiley, New York, 1981.
[37] H. Uslu, S. Altindal, U. Aydemir, I. Dokme, I.M. Afandiyeva, J. Alloys Compd. 503 (2010) 96–102.
[38] H. Uslu, S. Altindal, I. Dokme, J. Appl. Phys. 108 (2010) 104501.